# Alfvén Waves in the Lower Solar Atmosphere

David B. Jess, *et al.*

*Science* **323**, 1582 (2009);
DOI: 10.1126/science.1168680



*Science* (print ISSN 0036-8075; online ISSN 1095-9203) is published weekly, except the last week in December, by the American Association for the Advancement of Science, 1200 New York Avenue NW, Washington, DC 20005. 

in dopamine-depleted animals and an increased entrainment of spikes to low-frequency components of the LFPs. Such synchronous activity interferes with normal information processing in these circuits and should likely be considered pathogenic in PD (*12*). Our data show that DCS effectively abolishes aberrant synchronous low-frequency oscillations. It is, therefore, tempting to speculate that the suppression of low-frequency oscillations is particularly important for amelioration of motor symptoms in PD (*31*).

Finally, the combined effect of L-dopa and DCS allowed for recovery of motor function at significantly lower doses of L-dopa in severely dopamine-depleted animals. The considerably less invasive nature of the epidural DCS electrode compared with DBS electrodes suggests that DCS could be a complement for treatment of symptoms of PD in earlier stages of the disease. We therefore propose that DCS should be investigated further in extensive experiments employing primate models of PD, preferably over longer time periods, to evaluate the potential viability of this new procedure as a treatment for Parkinsonian patients.

### References and Notes


1. S. Fahn, *Ann. N.Y. Acad. Sci.* **991**, 1 (2003).
2. A. Carlsson, *Acta Neurol. Scand. Suppl.* **51**, 11 (1972).
3. O. Hornykiewicz, *Amino Acids* **23**, 65 (2002).
4. K. M. Shaw, A. J. Lees, G. M. Stern, *Q. J. Med.* **49**, 283 (1980).
5. A. L. Benabid, *Curr. Opin. Neurobiol.* **13**, 696 (2003).
6. J. S. Perlmutter, J. W. Mink, *Annu. Rev. Neurosci.* **29**, 229 (2006).
7. P. Plaha, Y. Ben-Shlomo, N. K. Patel, S. S. Gill, *Brain* **129**, 1732 (2006).
8. E. E. Fanselow, A. P. Reid, M. A. Nicolelis, *J. Neurosci.* **20**, 8160 (2000).
9. C. M. DeGiorgio, A. Shewmon, D. Murray, T. Whitehurst, *Epilepsia* **47**, 1213 (2006).
10. M. S. George *et al.*, *Biol. Psychiatry* **47**, 287 (2000).
11. P. Brown *et al.*, *J. Neurosci.* **21**, 1033 (2001).
12. C. Hammond, H. Bergman, P. Brown, *Trends Neurosci.* **30**, 357 (2007).
13. R. M. Costa *et al.*, *Neuron* **52**, 359 (2006).
14. T. D. Sotnikova *et al.*, *PLoS Biol.* **3**, e271 (2005).
15. D. J. Brooks, P. Piccini, *Biol. Psychiatry* **59**, 908 (2006).
16. K. G. Lloyd, L. Davidson, O. Hornykiewicz, *J. Pharmacol. Exp. Ther.* **195**, 453 (1975).
17. X. Drouot *et al.*, *Neuron* **44**, 769 (2004).
18. K. Sakai, D. M. Gash, *Brain Res.* **633**, 144 (1994).
19. Materials and methods are available as supporting material on *Science* Online.
20. M. A. Cenci, I. Q. Whishaw, T. Schallert, *Nat. Rev. Neurosci.* **3**, 574 (2002).
21. C. Winkler, D. Kirik, A. Bjorklund, M. A. Cenci, *Neurobiol. Dis.* **10**, 165 (2002).
22. I. Schlesinger, I. Erikh, D. Yarnitsky, *Mov. Disord.* **22**, 2394 (2007).
23. M. Glickstein, J. Stein, *Trends Neurosci.* **14**, 480 (1991).
24. P. D. Wall, *Brain* **93**, 505 (1970).
25. S. Grillner, P. Wallen, K. Saitoh, A. Kozlov, B. Robertson, *Brain Res. Brain Res. Rev.* **57**, 2 (2008).
26. S. M. Brudzynski, M. Wu, G. J. Mogenson, *Can. J. Physiol. Pharmacol.* **71**, 394 (1993).
27. M. R. DeLong, *Trends Neurosci.* **13**, 281 (1990).
28. Y. Smith, D. V. Raju, J. F. Pare, M. Sidibe, *Trends Neurosci.* **27**, 520 (2004).
29. C. J. Wilson, *Neuron* **45**, 575 (2005).
30. J. D. Berke, M. Okatan, J. Skurski, H. B. Eichenbaum, *Neuron* **43**, 883 (2004).
31. A. A. Kuhn *et al.*, *Brain* **127**, 735 (2004).


32. We thank W. M. Chan, G. Lehew, and J. Meloy for outstanding technical assistance; R. Gainetdinov, S.-C. Lin, H. Zhang, and K. Dzirasa for valuable comments; and S. Halkiotis for proofreading the manuscript. This work was supported by the National Institute of Neurological Disorders and Stroke (NINDS) R33NS049534 and the International Neuroscience Network Foundation to M.A.L.N., R01NS019576 and R01MH073853 to M.G.C., Ruth K. Broad Postdoctoral Award to R.F., and NRC and Knut and Alice Wallenberg Foundation to P.P. The content is solely the responsibility of the authors and does not necessarily represent the official views of the NINDS or the National Institutes of Health. M.A.L.N. dedicates this paper to Lily Safra for her continuing support and to the memory of his grandfather, Angelo Nicolelis, who suffered from Parkinson's disease. M.A.L.N. acknowledges a visiting professorship, Chaire Blaise Pascal, from the Région Ile de France at the Ecole Supérieure de Physique et de Chimie Industrielles, Paris.


### Supporting Online Material

www.sciencemag.org/cgi/content/full/323/5921/1578/DC1
Materials and Methods
Figs. S1 to S9
Movie S1
References


20 August 2008; accepted 10 December 2008
10.1126/science.1164901


REPORTS

# Alfvén Waves in the Lower Solar Atmosphere


**David B. Jess,[1,2]* Mihalis Mathioudakis,[1] Robert Erdélyi,[3] Philip J. Crockett,[1] Francis P. Keenan,[1] Damian J. Christian[4]**



**The flow of energy through the solar atmosphere and the heating of the Sun's outer regions are still not understood. Here, we report the detection of oscillatory phenomena associated with a large bright-point group that is 430,000 square kilometers in area and located near the solar disk center. Wavelet analysis reveals full-width half-maximum oscillations with periodicities ranging from 126 to 700 seconds originating above the bright point and significance levels exceeding 99%. These oscillations, 2.6 kilometers per second in amplitude, are coupled with chromospheric line-of-sight Doppler velocities with an average blue shift of 23 kilometers per second. A lack of cospatial intensity oscillations and transversal displacements rules out the presence of magneto-acoustic wave modes. The oscillations are a signature of Alfvén waves produced by a torsional twist of ±22 degrees. A phase shift of 180 degrees across the diameter of the bright point suggests that these torsional Alfvén oscillations are induced globally throughout the entire brightening. The energy flux associated with this wave mode is sufficient to heat the solar corona.**


Solar observations from both ground-based and spaceborne facilities show that a wide range of magneto-acoustic waves (*1*, *2*) propagate throughout the solar atmosphere. However, the energy they carry to the outer solar atmosphere is not sufficient to heat it (*3*). Alfvén waves (pure magnetic waves), which are incompressible and can penetrate through the stratified solar atmosphere without being reflected (*4*), are the most promising wave mechanism to explain the heating of the Sun's outer regions.

However, it has been suggested that their previous detection in the solar corona (*5*) and upper chromosphere (*6*) is inconsistent with magneto-hydrodynamic (MHD) wave theory (*7*, *8*). These observations are best interpreted as a guided-kink magneto-acoustic mode, whereby the observational signatures are usually swaying, transversal, periodic motions of the magnetic flux tubes (*7*, *9*). Numerical simulations (*10*) show that subsurface acoustic drivers and fast magneto-sonic kink waves (*11*, *12*) can convert energy into upwardly propagating Alfvén waves, which are emitted from the solar surface. These numerical simulations are also in agreement with current analytical studies. In particular, it has been shown that footpoint motions in an axially symmetric system can excite torsional Alfvén waves (*13*). Other Alfvén wave modes may exist, although these are normally coupled to magneto-sonic MHD waves (*14*). In the solar atmosphere, magnetic field lines clump into tight bundles, forming flux tubes. Alfvén waves in flux tubes could manifest as torsional oscillations (*7*) that create simultaneous blue and red shifts, leading to the non-thermal broadening of any isolated line profile, and should thus be observed as full-width half-maximum (FWHM) oscillations (*15*). A promising location for the detection of Alfvén waves is


[1]Astrophysics Research Centre, School of Mathematics and Physics, Queen's University, Belfast, BT7 1NN, Northern Ireland, UK. [2]Solar Physics Laboratory, NASA Goddard Space Flight Center, Code 671, Greenbelt, MD 20771, USA. [3]Solar Physics and Space Plasma Research Centre, University of Sheffield, Hicks Building, Hounsfield Road, Sheffield, S3 7RH, England, UK. [4]Department of Physics and Astronomy, California State University Northridge, 18111 Nordhoff Street, Northridge, CA 91330, USA.

*To whom correspondence should be addressed. E-mail: d.jess@qub.ac.uk

in the lower solar atmosphere, where they can be generated by the overshooting of convective motions in the photosphere (*16*). Here, we report the detection of substantially blue-shifted plasma and FWHM oscillations originating in a large conglomeration of magnetic bright points.

We used the Swedish Solar Telescope (SST) to image a 68-by-68–arc sec region on the solar surface positioned near the disk center. Using the Solar Optical Universal Polarimeter (SOUP) (*17*) and high-order adaptive optics (*18*), we obtained narrowband images across the Hα absorption profile centered at 6562.8 Å. We observed with a cadence of 0.03 s to obtain 89 min of uninterrupted data. Because SOUP is tunable, we sampled the complete Hα line profile using seven discrete steps. The wavelength intervals we chose became increasingly narrow toward the line core in order to enable an accurate determination of the line characteristics, such as Doppler velocities, FWHMs, and intensities. Our images have a sampling of 0.068 arc sec per pixel, which corresponds to ≈110-km resolution (two pixels) on the solar surface.

By using the multi-object multi-frame blind deconvolution (MOMFBD) (*19*) image restoration technique to remove the small-scale atmospheric distortions present in the data, we achieved an effective cadence of 63 s for a full line profile. We acquired 85 complete scans across the Hα line profile in addition to 595 simultaneous continuum images. For each of the 85 profile scans, every pixel of the 1024-by-1024–pixel$^2$ charge-coupled device contains information acquired at a particular wavelength position. Therefore, we obtained a total of $8.9 \times 10^7$ individual Hα absorption profiles, covering the full 68-by-68–arc sec field of view, during the 89-min duration of the data set. We fit a Gaussian distribution to each of the observed Hα profiles to obtain values for the integrated intensity and FWHM. To determine the line-of-sight velocity, we compared each measured central wavelength position with the rest-frame Hα profile core at 6562.8 Å. We created time series for intensity, line-of-sight velocity, FWHM, and wavelength-integrated data cubes and used fast Fourier transform and wavelet routines to analyze them.

The SST field of view shows a range of features, including pores, exploding granules, and a multitude of bright points (Fig. 1), a large conglomeration of which is located at heliocentric coordinates (–10 arc sec, 10 arc sec) or N07E01 in the solar north-south–east-west coordinate system. We selected a 10-by-10–arc sec box surrounding the bright-point group (BPG), which occupies an area of 430,000 km$^2$, for

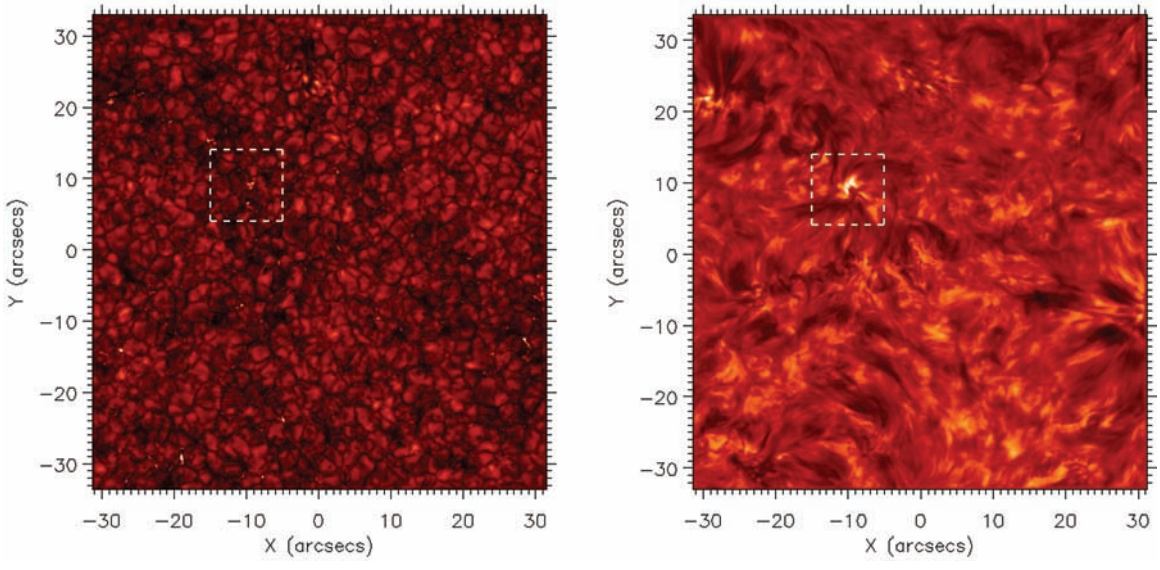


**Fig. 1.** Simultaneous images in the (**left**) Hα continuum (photosphere) and (**right**) Hα core (chromosphere) obtained with the SST. The conglomeration of bright points within the region we investigated is denoted by a square of dashed lines. The scale is in heliocentric coordinates where 1 arc sec ≈ 725 km.

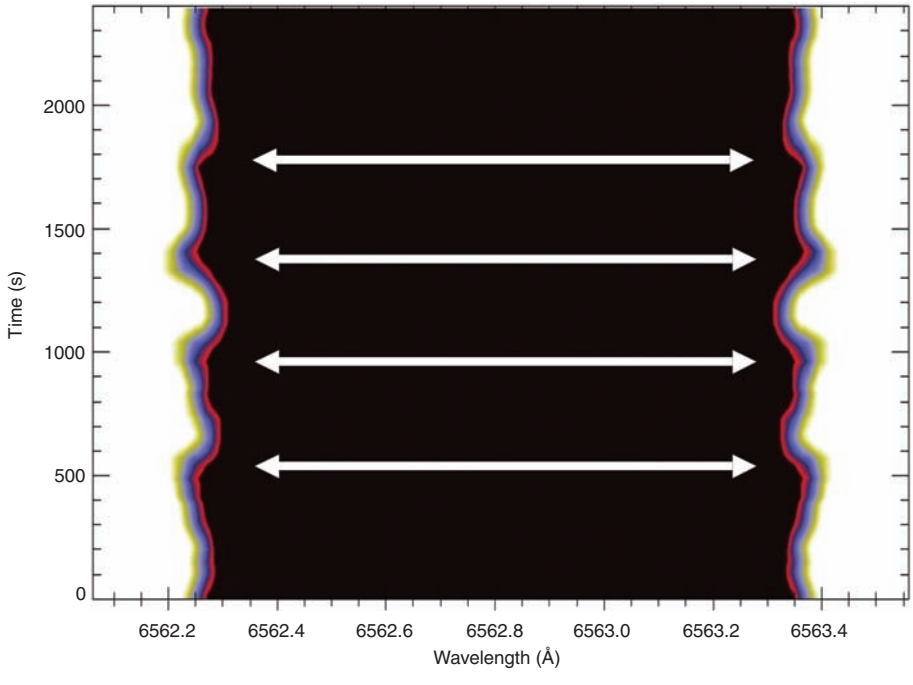


**Fig. 2.** A wavelength-versus-time plot of the Hα profile showing the variation of line width at FWHM as a function of time. The arrows indicate the positions of maximum amplitude of a 420-s periodicity associated with the bright-point group located at (–10 arc sec, 10 arc sec) in Fig. 1. The torsional motion of the Alfvénic perturbations creates nonthermal broadening that is visible in the Hα line profile. The peak-to-peak velocity is ≈3.0 km s$^{-1}$ (≈65 mÅ). For an inclination angle of 35°, the absolute velocity amplitude is ≈2.6 km s$^{-1}$.

further investigation. The line-of-sight Doppler velocities associated with this BPG show blue shifts with an average value of 23 km $s^{-1}$. There is no evidence of periodic trends in either intensity or line-of-sight velocity; the intensity of the BPG is constant, with minimal variation during its 53-min lifetime.

Wavelet analysis shows that FWHM oscillations with significance levels exceeding 99% occur within the spatially averaged BPG (Fig. 2). We detected FWHM oscillations as low as the Nyquist period (126 s) throughout the duration of the data set, with the strongest detected power originating in the 400-to-500-s interval. These oscillations are located directly above the large BPG, encompassing a near-circular shape that is cospatial with the detected Doppler velocities, and are apparent in all FWHM time series. This shows that powerful coherent periodicities are present throughout the surface of the BPG. We detected oscillations until the BPG fragmented into a series of smaller bright points after 3150 s.

Numerical simulations based on three-dimensional magnetoconvection show that the bright points that were observed in the wing of the Hα line profile correspond to magnetic field concentrations measured in kilogauss in the photosphere (*20*). The canopy structure seen in the Hα core images reveals a wealth of flux-tube structures, with many securing anchor positions in the photosphere directly above the BPG (Fig. 1). The coincidence of bright-point structures with high magnetic field concentrations implies that MHD waves are likely to be present (*21*). However, the chromospheric brightening is of much larger physical size than the underlying photospheric BPG. Because the observations were made very close to the center of the solar disk, an increase in physical size between the photosphere and the chromosphere can be interpreted as an expansion of the photospheric flux-tube bundle as a function of atmospheric height (*22*). A comparison of the maximum diameter of the bright point at each height in the atmosphere suggests an expansion of ~1300 km; a height separation of ≈1000 km and a symmetric expansion around the bright-point center suggest a flux-tube expansion angle of ≈33°. Additionally, an offset of ≈700 km between the centres of the BPG at photospheric and chromospheric heights suggests a magnetic flux-tube tilt angle of ≈35° from the vertical.

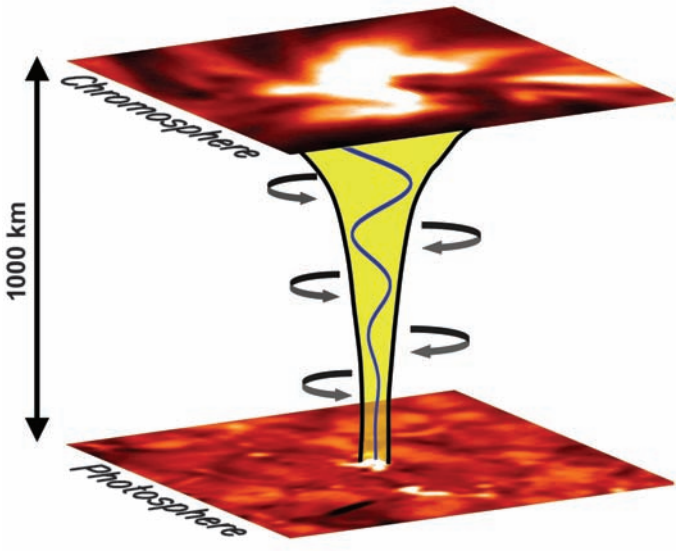


**Fig. 3.** Expanding magnetic flux tube sandwiched between photospheric and chromospheric intensity images obtained with the SST, undergoing a torsional Alfvénic perturbation and generating a wave that propagates longitudinally in the vertical direction. At a given position along the flux tube, the Alfvénic displacements are torsional oscillations that remain perpendicular to the direction of propagation and magnetic field outlining constant magnetic surfaces. The largest FWHM will be produced when the torsional velocity is at its maximum (at zero displacement from the equilibrium position). The figure is not to scale.

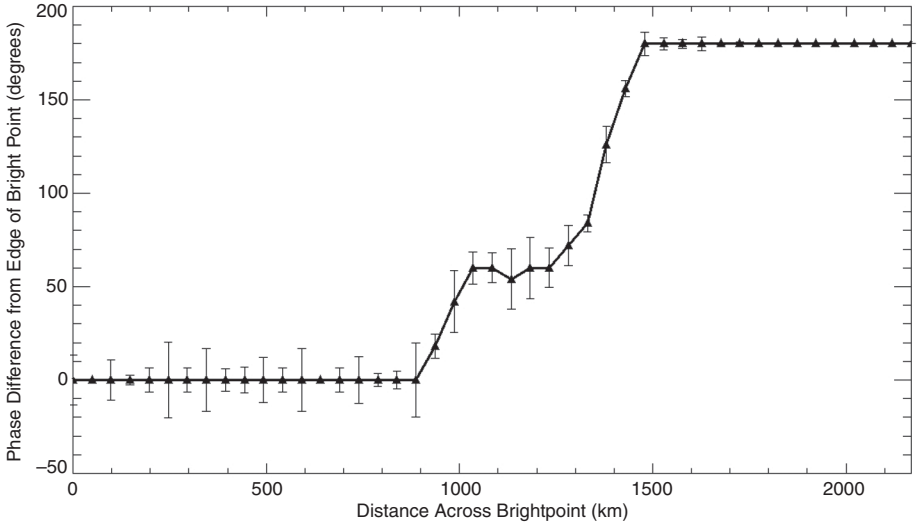


**Fig. 4.** Average phase difference of FWHM oscillations plotted as a function of distance across the diameter of the bright point. The triangles denote the locations where a measurement is made, and the error bars indicate the phase variance in the temporal domain. The phase at 0 km is used as a reference, with all other phases plotted relative to this value. Spatial coherence of FWHM oscillations across the BPG ranges between 90 and 100%, suggesting that the BPG is acting as a coherent waveguide. The phase difference increases around the midpoint of the BPG with opposite sides of the waveguide, indicating out-of-phase oscillatory phenomena, which is as predicted for a torsional Alfvénic perturbation.

Alfvénic fluxes are predicted to be at their strongest in the regime of high magnetic field strength and moderately inclined waveguides (*10*). Because of their incompressibility, they exhibit no periodic intensity perturbations. Thus, the observational signature of a torsional Alfvén wave propagating with a velocity component along the observer's line of sight will arise from its torsional velocities on small spatial scales (*8*). These torsional velocities are responsible for the FWHM oscillations we observed (Fig. 3). The line-of-sight velocity amplitude of ≈1.5 km $s^{-1}$ and the inclination angle of ≈35° indicate an absolute Alfvénic perturbation amplitude of ≈2.6 km $s^{-1}$. Because the circumference of the photospheric bright point [where torsional Alfvén waves are believed to be generated (*16*)] is on the order of 2800 km (55 pixels), a torsional twist of ±22° is sufficient to generate the observed wave motion.

The moderate inclination angle of the flux tubes, coupled with the detection of substantially blue-shifted material and strong FWHM oscillations, is evidence of the presence of torsional Alfvén waves. For a typical photospheric internal waveguide electron density (*23*) of $n_e^i \approx 10^{16}$ $cm^{-3}$ and a magnetic field strength (*20*) of 1000 G, the Alfvén speed within a cylindrical flux tube is estimated (*14*) to be ≈22 km $s^{-1}$. This value is above the speed of sound in the upper photosphere/lower chromosphere (*24*) and is consistent with the blue-shift velocity we determined.

We took a slice through the center of the bright point and analyzed the stability of opposite edges of the BPG as a function of time. This was performed by examining any displacements of the BPG from its initial position at the start of the observing sequence (fig. S1). The bright point moves less than one pixel during the first 3150 s. As the BPG begins to fragment after 3150 s, the motions of the bright-point edges increase substantially. However, we did not find periodic motions of the bright point, particularly during the initial 3150 s when the FWHM oscillations were detected. A magneto-acoustic wave mode would produce ob-

servable periodicities in intensity, similar to those caused by the periodic contractions when viewed along the flux tube, that are associated with sausage-mode waves (*25*). A sausage-mode wave is caused by the axially symmetric expansion and contraction of magnetic flux tubes (*14*). Kink-mode oscillations are generated through a bulk motion, whereby the whole flux tube is displaced from its original position in a periodic fashion. Therefore, magneto-acoustic waves cannot explain our observations.

A torsional Alfvénic perturbation should produce a FWHM oscillation that is 180° out of phase at opposite boundaries of the waveguide (*8*). The relative time-averaged oscillatory phase as a function of distance across the ≈2200-km diameter of the bright point shows that opposite sides of the bright point display oscillatory phenomena that are indeed 180° out of phase (Fig. 4). This is consistent with current torsional Alfvénic wave models (*26*).

We estimated the energy flux of the observed waves using $E = \rho v^2 v_A$, where ρ is the mass density of the flux-tube, $v$ is the observed velocity amplitude, and $v_A$ is the Alfvén speed (*6*). For a mass density of $\rho \approx 1 \times 10^{-6}$ kg m$^{-3}$, derived from a quiet-Sun chromospheric model (*23*), the energy flux in the chromosphere is $E \approx 15000$ W m$^{-2}$. At any one time, it is estimated (*27*) that at least 1.6% of the solar surface is covered by BPGs similar to that presented here. Thus, combining the energy carried by similar BPGs over the entire solar surface produces a global average of 240 W m$^{-2}$. Alfvén waves with an energy flux of ≈100 W m$^{-2}$ are believed to be vigorous enough to heat the localized corona or to launch the solar wind when their energy is thermalized (*6*, *28*). Therefore, a transmission coefficient of ≈42% through the thin transition region will provide sufficient energy to heat the entire corona. Regions containing highly magnetic structures, such as bright points, should possess even higher mass densities (*29*). In this regime, the energy flux available to heat the corona will be substantially higher than the minimum value required to sustain localized heating.

### References and Notes


1. Magneto-acoustic waves, normally classified as fast and slow, are waves of acoustic origin whose properties are modified by the presence of a magnetic field.
2. V. M. Nakariakov, E. Verwichte, *Living Rev. Sol. Phys.* **2**, 3 (2005).
3. A. Fossum, M. Carlsson, *Nature* **435**, 919 (2005).
4. L. Ofman, *Astrophys. J.* **568**, L135 (2002).
5. S. Tomczyk *et al.*, *Science* **317**, 1192 (2007).
6. B. De Pontieu *et al.*, *Science* **318**, 1574 (2007).
7. R. Erdélyi, V. Fedun, *Science* **318**, 1572 (2007).
8. T. Van Doorsselaere, V. Nakariakov, E. Verwichte, *Astrophys. J.* **676**, L73 (2008).
9. V. Kukhianidze, T. V. Zaqarashvili, E. Khutsishvili, *Astron. Astrophys.* **449**, L35 (2006).
10. P. S. Cally, M. Goossens, *Sol. Phys.* **251**, 251 (2008).
11. M. Goossens, I. Arregui, J. L. Ballester, T. J. Wang, *Astron. Astrophys.* **484**, 851 (2008).
12. W. J. Tirry, M. Goossens, *Astrophys. J.* **471**, 501 (1996).
13. M. S. Ruderman, D. Berghmans, M. Goossens, S. Poedts, *Astron. Astrophys.* **320**, 305 (1997).
14. P. M. Edwin, B. Roberts, *Sol. Phys.* **88**, 179 (1983).
15. T. V. Zaqarashvili, *Astron. Astrophys.* **399**, L15 (2003).
16. J. Vranjes, S. Poedts, B. P. Pandey, B. De Pontieu, *Astron. Astrophys.* **478**, 553 (2008).
17. A. M. Title, W. J. Rosenberg, *Opt. Eng.* **20**, 815 (1981).
18. G. B. Scharmer, P. M. Dettori, M. G. Lofdahl, M. Shand, *Proc. SPIE* **4853**, 370 (2003).
19. M. van Noort, L. H. M. Rouppe van der Voort, M. G. Lofdahl, *Sol. Phys.* **228**, 191 (2005).
20. J. Leenaarts, R. J. Rutten, P. Sütterlin, M. Carlsson, H. Uitenbroek, *Astron. Astrophys.* **449**, 1209 (2006).
21. W. Kalkofen, *Astrophys. J.* **486**, L145 (1997).
22. S. K. Solanki, W. Finsterle, I. Ruedi, W. Livingston, *Astron. Astrophys.* **347**, L27 (1999).
23. J. E. Vernazza, E. H. Avrett, R. Loeser, *Astrophys. J. Suppl.* **45**, 635 (1981).
24. B. Sánchez-Andrade Nũno, N. Bello González, J. Blanco Rodriguez, F. Kneer, K. G. Puschmann, *Astron. Astrophys.* **486**, 577 (2008).
25. V. M. Nakariakov, V. F. Melnikov, V. E. Reznikova, *Astron. Astrophys.* **412**, L7 (2003).
26. P. Copil, Y. Voitenko, M. Goossens, *Astron. Astrophys.* **478**, 921 (2008).
27. D. S. Brown, C. E. Parnell, E. E. Deluca, L. Golub, R. A. McMullen, *Sol. Phys.* **201**, 305 (2001).
28. A. Verdini, M. Velli, *Astrophys. J.* **662**, 669 (2007).
29. D. Pérez-Suárez, R. C. Maclean, J. G. Doyle, M. S. Madjarska, *Astron. Astrophys.* **492**, 575 (2008).



30. D.B.J. is supported by a Northern Ireland Department for Employment and Learning studentship and thanks NASA Goddard Space Flight Center for a Co-operative Award in Science and Technology studentship. R.E. thanks M. Kéray for encouragement and is grateful to NSF, Hungary (Országos Tudományos Kutatási Alapprogram, ref. no. K67746), for financial support. F.P.K. is grateful to the Atomic Weapons Establishment–Aldermaston for the award of a William Penney Fellowship. The SST is operated on the island of La Palma by the Institute for Solar Physics of the Royal Swedish Academy of Sciences in the Spanish Observatorio del Roque de los Muchachos of the Instituto de Astrofísica de Canarias. These observations have been funded by the Optical Infrared Coordination network, an international collaboration supported by the Research Infrastructures Programme of the European Commission's Sixth Framework Programme. This work is supported by the Science and Technology Facilities Council, and we thank L. H. M. Rouppe van der Voort for help with MOMFBD image processing.


### Supporting Online Material

www.sciencemag.org/cgi/content/full/323/5921/1582/DC1
Fig. S1


18 November 2008; accepted 27 January 2009
10.1126/science.1168680


# The Disorder-Free Non-BCS Superconductor $Cs_3C_{60}$ Emerges from an Antiferromagnetic Insulator Parent State


**Yasuhiro Takabayashi,[1]* Alexey Y. Ganin,[2]* Peter Jeglič,[3] Denis Arčon,[3,4] Takumi Takano,[5] Yoshihiro Iwasa,[5] Yasuo Ohishi,[6] Masaki Takata,[6,7] Nao Takeshita,[8] Kosmas Prassides,[1]† Matthew J. Rosseinsky[2]†**



The body-centered cubic A15-structured cesium fulleride $Cs_3C_{60}$ is not superconducting at ambient pressure and is free from disorder, unlike the well-studied face-centered cubic $A_3C_{60}$ alkali metal fulleride superconductors. We found that in $Cs_3C_{60}$, where the molecular valences are precisely assigned, the superconducting state at 38 kelvin emerges directly from a localized electron antiferromagnetic insulating state with the application of pressure. This transition maintains the threefold degeneracy of the active orbitals in both competing electronic states; it is thus a purely electronic transition to a superconducting state, with a dependence of the transition temperature on pressure-induced changes of anion packing density that is not explicable by Bardeen-Cooper-Schrieffer (BCS) theory.


Superconductivity requires an attractive interaction between electrons to form Cooper pairs, which form a condensate that can move without electrical resistance. In simple metals and alloys, the Bardeen-Cooper-Schrieffer (BCS) theory explains how electron-phonon coupling overcomes the repulsion between negatively charged electrons (*1*). In high-temperature superconductors, such as the copper oxides and iron oxyarsenides, the origin of the attraction is less clear. Beyond the theoretical challenges, the experiments are complicated by imperfections within the materials, such as structural disorder, low symmetry and dimensionality, and variations in chemical valence at the electronically active sites. Here we show that in the cubic alkali metal fulleride $Cs_3C_{60}$, which is completely ordered and for which precise valences can be assigned, the 38 K superconducting state (*2*) emerges directly from a localized electron antiferromagnetic insulating (AFI) state with the application of pressure as the anion packing density increases. This transition maintains the threefold degeneracy of the active orbitals in both competing electronic states, and is thus a purely electronic transition to a superconducting state. The transition temperature $T_c$ depends on the anion packing density in a way that is not explicable within a simple BCS approach.

In systems where the bands in which the electrons move are narrow, there are electron-electron correlation energies associated with inter-electron repulsion, which are comparable to the electronic bandwidth. These electron correlation effects (*3*) need to be taken into account in understanding the mechanisms for formation of the Cooper pairs (*4*). These concepts have been developed primarily in d-electron–based systems